

The role of the cytoskeleton in volume regulation and beading transitions in PC12 neurites

Pablo Fernández* and Pramod A. Pullarkat†

* E27 Lehrstuhl für Zellbiophysik, Technische Universität München
James Franck Straße, D-85748 Garching, Germany
pfernand@ph.tum.de

† Raman Research Institute
C. V. Raman Avenue, Sadashivanagar, 560080 Bangalore, India
pramod@rri.res.in

November 11, 2021

Abstract

We present investigations on volume regulation and beading shape transitions in PC12 neurites conducted using a flow-chamber technique. By disrupting the cell cytoskeleton with specific drugs we investigate the role of its individual components in the volume regulation response. We find that microtubule disruption increases both swelling rate and maximum volume attained, but does not affect the ability of the neurite to recover its initial volume. In addition, investigation of axonal beading –also known as pearling instability– provides additional clues on the mechanical state of the neurite. We conclude that the initial swelling phase is mechanically slowed down by microtubules, while the volume recovery is driven by passive diffusion of osmolites. Our experiments provide a framework to investigate the role of cytoskeletal mechanics in volume homeostasis.

Keywords: Volume regulation, cell mechanics, axon beading, cytoskeleton.

PACS: 87.16.ln, 87.16.dp, 87.16.ad.

INTRODUCTION

The ability of living cells to regulate their volume is a ubiquitous homeostatic feature in biology (1, 2). Since water readily permeates through the cellular membrane, alterations in extracellular osmolarity can change the con-

centration of all cytoskeletal components with severe consequences for the metabolism. Not surprisingly, one finds several mechanisms involved in volume regulation. In particular, many eukaryotic cell types display a short-term volume regulation response to sudden alterations in external osmolarity, the so-called regulatory volume decrease (RVD) and regulatory volume increase (RVI) (2, 3). It is generally accepted that these require the passive diffusion of ions. In the case of RVD, cell swelling upon hypoosmotic shock increases the membrane permeability for sodium, which diffuses out of the cell. In turn, the decrease of intracellular osmolarity drives water out and lowers cell volume (2, 3). In this mechanism water flow is driven by a difference in osmotic pressure. It is often assumed that hydrostatic pressures are negligible (4), with the argument that they would make the membrane burst (1). However, though the maximal pressures sustained by lipid bilayers are indeed very low, the situation cannot be simply extrapolated to the living cell. The cell membrane is connected to the cytoskeleton, the biopolymer gel spanning across the cell interior (5–7). Since the cytoskeleton is viscoelastic and contractile (8–11) (also in PC12 neurites (12)), it may provide a mechanical memory of the initial state as well as a driving force for volume relaxation (13–20). Though it has been argued that the cytoskeleton is too weak (typical moduli are up to 10 kPa (8, 10)) to sustain osmotic pressures (up to \sim MPa) (7), neurons under hypoosmotic shock sustain strong pressures for several hours (21) and swelling of erythrocytes increases and approach perfect osmometer behaviour af-

ter disruption of the spectrin-actin cytoskeleton (22). This is indeed compelling evidence for a mechanical role, but in many systems the cytoskeleton seems to additionally play a signalling one. In particular, biochemical interactions between actin filaments and ion channels may couple strain of the actin cortex to changes in channel activity (2, 23). The fact that the actin cortex is disrupted when hypoosmotic swelling begins (24, 25) seems to be due to an influx of Ca^{2+} (26) through mechanosensitive ion channels activated by membrane stretching (27, 28). To clarify the role of the cytoskeleton one must discern between pure mechanical and mechanosensing responses, a difficult task requiring direct measurements of membrane tension.

In this work, we study volume regulation in neurites, axon-like cylindrical protrusions extended by PC12 cells (29), structurally very similar to the axons produced by neurons in culture (6, 30). Neurites furnish a hitherto unexplored, yet attractive model system to investigate the role of mechanical tension in volume regulation. Their simple cylindrical geometry and low amount of invaginated membrane allows better volume and area calculations from images. They also have a well-defined, highly organized cytoskeletal structure similar to that of axons: a central array of longitudinally arranged microtubules interconnected by microtubule binding proteins and surrounded by an actin cortex. Moreover, an exceptional feature of axons and neurites is their ability to undergo sudden shape transformations in response to an applied mechanical tension (20, 31, 32), an instability known as axonal beading to biologists and pearling instability to physicists. We show that axonal swelling increases membrane tension and that microtubules slow down the volume response. We conclude that frictional forces in the cytoskeleton play an important role in axonal volume regulation.

EXPERIMENTAL SETUP AND METHODS

Flow chamber

The experiments have been carried out using a flow-chamber technique. A schematic of the set-up is shown in Fig. 1. A stainless-steel block and two coverslips are used to form a $10 \times 5 \times 1 \text{ mm}^3$ chamber. Cells adhere on the bottom cover-slip. One duct of the chamber is connected to a peristaltic pump by means of long, soft silicone-rubber tubing that minimizes pressure fluctuations arising from the pump. The other duct is connected to a 3-way-valve

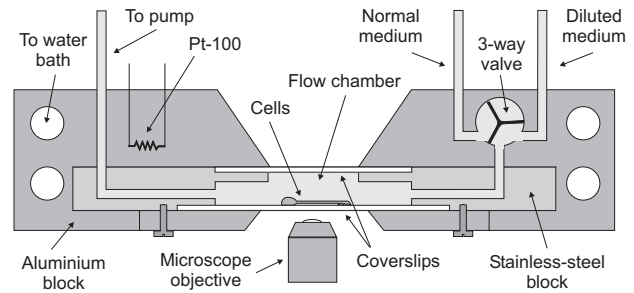


Figure 1: A schematic diagram of the flow-chamber set-up.

to select between two different media that can be pumped into the chamber. Stainless-steel tubes that are 1 mm in diameter connect the 3-way-valve to the two reservoirs where the media are stored. The chamber is intentionally made small to ensure a quick switching from one medium to the other at low flow rates, in the range of $2-4 \mu\text{l/s}$. The switching of concentrations inside the chamber was studied by adding an absorbing dye to one of the solutions and monitoring the variation in the transmitted intensity with time. The concentration reaches 90% of its final value in about 10 s. The chamber, the 3-way-valve, and the stainless-steel tubes are placed inside an aluminium block with good thermal contact between each other and a water bath maintains the temperature of the block at the desired value. The continuous flow of pre-warmed medium keeps the chamber at constant temperature despite some heat loss through the cover-slips.

Cell culture

PC12 cells are from the German Collection of Microorganisms and Cell Lines (DSMZ) (33). They are plated on collagen coated slides and cultured in RPMI-1640 medium (Gibco) with 10% fetal bovine serum and 5% horse serum in presence of nerve growth factor (NGF) (Sigma-Aldrich Chemie, Munich, Germany) for 4–5 days (34). Such young neurites are known not to have intermediate filaments (30). Slides are coated with 3-aminopropyl triethoxysilane (Sigma). The silanised slides are covered with about $100 \mu\text{l}$ of 10% rat-tail collagen (Sigma-Aldrich) dissolved in a 70% ethanol – 30% water solution and let dry overnight.

Experimental procedure

Prior to an experiment, the slide with the adherent cells is transferred to the flow-chamber. Cells are allowed to stabilize for about 5 min by circulating the experiment

medium (normal medium with addition of 25 mM HEPES buffer (Invitrogen, Darmstadt, Germany)). Experiments are performed by switching from the normal experiment medium to experiment medium diluted with deionized water. The response of the cells to the sudden switch in the external concentration is observed with an Axiovert 135 microscope (Zeiss, Oberkochen, Germany) configured for phase-contrast imaging.

Image analysis

The volume and area of the neurites are analyzed from the recordings using a home-made edge detection program. Edge detection using a threshold for intensity is unreliable due to the “halo effect” present in phase-contrast images and also due to the dependence on the illumination intensity. To avoid such complications, edge pixels are recognized along the neurite by detecting the local maxima in the gradient of intensity across the neurite. After edge detection the neurite volume and surface area are computed assuming axial symmetry for the neurite shape. Axial symmetry is verified by comparing the two detected boundaries of several neurites and is found to be a good approximation for straight neurites which are attached only at the two extremities. Only such neurites were selected for the experiments.

Drug-induced cytoskeletal perturbation

Experiments were performed in presence of cytoskeleton disrupting drugs in order to study the role of its individual components. A complication in these experiments arises due to the neurites becoming fragile or losing their cylindrical geometry on cytoskeletal perturbation. This precluded experiments with the actin disrupting drug Latrunculin, which induces detachment of the growth cone. In the case of the microtubule disrupting drug Nocodazole (NOC) (35), which induces shape irregularities after approximately 10 min exposure, we let the drug act for 5 min before performing the hypoosmotic shock. NOC concentration was 10 $\mu\text{g/ml}$ throughout. In contrast, the myosin-blocking drug Blebbistatin (36) did not significantly alter neurite shape. Thus, to ensure its effect we incubated neurites at 37° for 1 hour at a high concentration (50 μM) before transferring them to the experiment chamber and performing the experiment at a lower concentration of 20 μM . For all experiments, drugs were present both in the normal and in the diluted medium. Since all drugs are dissolved in dimethylsulfoxide (DMSO), which itself has effects on water and ion channels (37), we performed control experiments in presence of DMSO 0.5%,

equal to the highest DMSO concentration in any of the drug experiments.

EXPERIMENTAL RESULTS

Volume dynamics

We begin all experiments with a hypoosmotic shock imposed by switching the cell culture medium flowing through the chamber from normal medium with a total solute concentration $C_0 \simeq 300$ mM to a lower external value C_e (the continuous flow ensures constant external concentration at all times). In the following, for an intuitive measure of the shock strength we will normalize the external osmolarity by its initial value and denote it by $C = C_e/C_0$. Figure 2 shows typical responses for three different values of C at 36°C. For weak shocks ($C = 0.8$) the neurite volume increases from its initial volume V_0 until it reaches a maximum steady value V_{max} . No recovery is observed for tens of minutes. For intermediate shocks, $C = 0.7$, the volume increases at a roughly constant rate \dot{V}_0 initially until it reaches a maximum value V_{max} . Subsequently, the volume recovers almost back to V_0 with a typical regulatory volume decrease response (RVD). The volume recovery is roughly exponential with a characteristic time τ . The recovery time τ is strongly temperature-dependent (shown later), but does not follow a clear trend with neurite diameter. For strong shocks, $C = 0.5$, the recovery is faster and there is often a remarkable “undershoot”, where the volume goes below its initial value. Moreover, during the swelling phase the neurite undergoes a sudden and transient shape transformation from its normal cylindrical geometry to a periodically modulated one. As discussed later, this Rayleigh-like “pearling” instability or beading indicates an increase in membrane tension upon neurite swelling. This shape transformation, which will be discussed later, does not affect the volume response curve in any measurable way. This fact allow us to discuss the volume dynamics and shape dynamics in that order.

Once the volume stabilizes to the lower external osmolarity C_e (within about ten minutes), we perform a hyperosmotic shock by switching back the original medium with concentration C_0 . The neurite shrinks, reaches a minimum volume V_{min} and then comes back to its initial volume in an RVI response as shown in Fig. 2. No beading shape transformation is observed in this case.

In the following, we separately address the volume regulation response and the peristaltic modulation. We study them as a function of osmotic shock strength, tempera-

ture, and in the presence of cytoskeleton-disrupting drugs.

Nonlinear swelling response. Figure 3 A shows the initial rate of change of volume divided by the initial area, \dot{V}_0/A_0 , as a function of the initial osmotic pressure difference $\Delta\Pi_0 = RTC_0(1 - C)$, for temperatures 33–36°C. Assuming zero hydrostatic pressure and neglecting changes in internal osmolarity gives the following expression for the initial swelling rate:

$$\dot{V}_0 = A_0 L_p \Delta\Pi_0, \quad (1)$$

where L_p is the hydraulic permeability. Surprisingly, from the average \dot{V}_0 value at $C = 0.7$ we obtain an osmotic permeability $P_f = RT\delta_W L_p \simeq 1.4 \mu\text{m/s}$ (where δ_W is the molar density of water), which is about two orders of magnitude lower than the literature values for lipidic membranes and most biological cells (1, 38–40) even after blockage of water channels (37). Moreover, as can be seen from Fig. 3 A, the expected linear dependence is contradicted by the strong nonlinear response observed for both hypo- and hyperosmotic shocks.

We now turn to the maximum (minimum) volume attained in a hypoosmotic (hyperosmotic) shock. The maximum (minimum) volume V_{max} (V_{min}) is to a good approximation proportional to the initial volume V_0 and does not depend significantly on the temperature (data not shown (41)). Thus we look at the relative maximum volume V_{max}/V_0 in order to minimize the effect of neurite diameter. As shown in Fig. 3 B, the maximum volume increases nonlinearly with the initial osmotic pressure difference $\Delta\Pi_0$. The data is contrasted to the perfect osmometer equation, corresponding to a constant total amount of internal osmolytes and zero hydrostatic pressure:

$$\frac{V_0 - V_{\text{dead}}}{V_{\text{max}} - V_{\text{dead}}} = C, \quad (2)$$

where the dead volume V_{dead} represents non-aqueous internal volume. Mammalian cells have on the average a cytosolic protein concentration of $\sim 20\%$ (5). According to electron microscopy studies (30) the non-cytosolic volume of PC12 neurite is comprised mostly of microtubules and organelles and amounts to $V_{\text{dead}} \simeq 25\% V_0$. The black region in Fig. 3 B corresponds to $V > V_0/C$ for hypoosmotic shocks and to $V < V_0/C$ for hyperosmotic shocks; penetrating this region would require work against the osmotic gradient. As expected for a passive response, the data lies outside them. For mild shocks, $C \geq 0.7$ and (hyperosmotic) $C \leq 1.4$, neurites swell as much as perfect osmometers a dead volume of 25%. Therefore, any ion leakage or hydrostatic pressure are negligible during the swelling phase. However, at strong

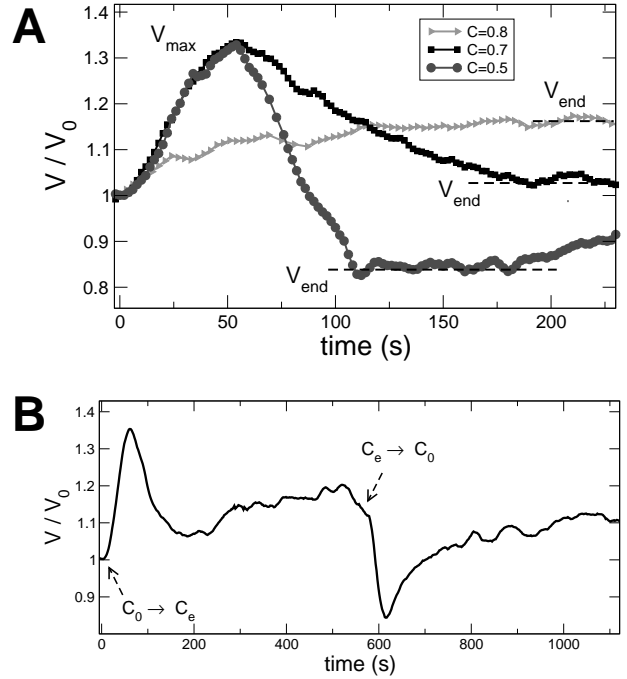


Figure 2: **A:** Swelling and recovery after a hypoosmotic shock performed at time $t = 0$. Normalised volume V/V_0 as a function of time for different dilutions: $C = 0.5$, (circles), $C = 0.7$ (solid line), $C = 0.8$ (dashed line). Temperature is in all cases 36°C. Each curve corresponds to a different neurite. The maximum volume attained is V_{max} , and the minimum is V_{end} . Notice the strong undershoot of the volume at $C = 0.5$, and the absence of recovery at $C = 0.8$. These are all general trends of the volume response. **B:** The full observed response when the neurite is subjected to a hypoosmotic shock and a subsequent hyperosmotic shock. At first the hypoosmotic shock $C_0 \rightarrow C_e$ is applied and the neurite is allowed to swell and relax (RVD). After the relaxation phase the hyperosmotic shock $C_e \rightarrow C_0$ is applied and the neurite shrinks and recovers the initial volume (RVI). Such $C_0 \rightarrow C_e \rightarrow C_0$ cycles can be repeated up to five times in a given neurite before the ends detach (data not shown).

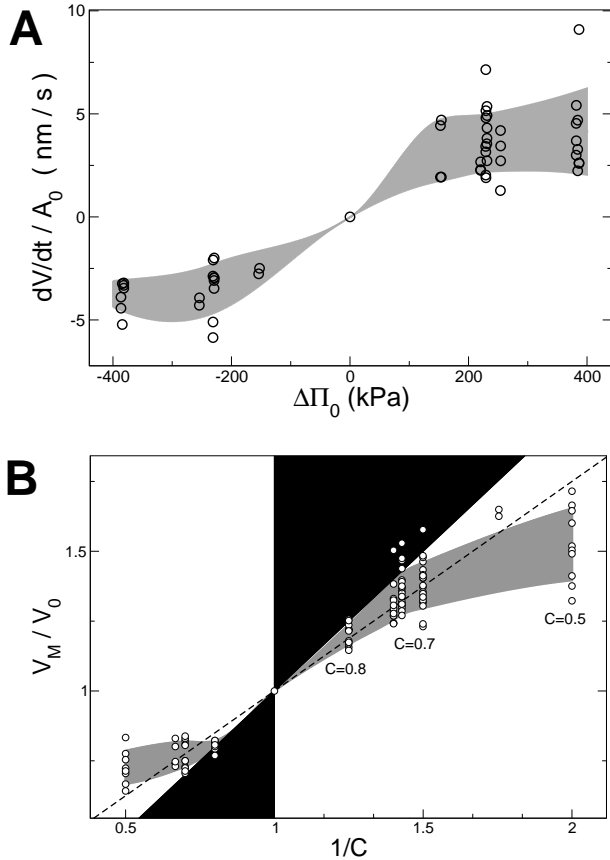


Figure 3: **A:** Initial swelling speed \dot{V}_0/A_0 as a function of the initial osmotic pressure difference $\Delta\Pi_0$ for temperatures 33 – 36°C. The shaded region is a guide to the eye, a spline going through the averages within a standard deviation. Notice the nonlinear response to strong hypo- as well as hyperosmotic shocks. **B:** Maximum change in relative volume V_M/V_0 as a function of the inverse external concentration $1/C$, for all temperatures (here V_M stands for V_{max} or V_{min} as the case may be). The grey region is a guide to the eye. The dashed line corresponds to a perfect osmometer with dead volume $V_{dead} = 0.25V_0$, and the black regions correspond to negative dead volumes.

shocks (hypoosmotic $C = 0.5$ or hyperosmotic $C = 2$), neurites swell significantly less than a perfect osmometer would. Thus, upon strong osmotic perturbations either ions leak or a sustained hydrostatic pressure develops.

Volume regulation under cytoskeleton disruption.

The axonal cytoskeleton may be expected to contribute to the volume response in several ways. As discussed in the introduction, a mechanical as well as a signalling role is conceivable. In order to assess the role of individual components of the cytoskeleton, we treat neurites with the myosin blocking drug Blebbistatin (BLE) (36) and the microtubule disrupting drug Nocodazole (NOC) (35). Since these are all diluted in dimethylsulfoxide (DMSO), a compound known to alter ion channels, we also perform control experiments in presence of DMSO.

Fig. 4 A shows typical responses. In presence of Nocodazole the initial swelling rate for strong shocks $C = 0.5$, increases markedly, but it barely changes for $C = 0.7$ (see Fig. 4 B). With Blebbistatin we observe a weaker but still significant effect. For both drugs, the relationship between swelling rate and initial osmotic pressure difference approaches the naively expected linear dependence given by Eq. 1.

Nocodazole induced disruption of microtubules also has a strong effect on the maximum volume V_{max} attained after a strong shock of $C = 0.5$, as shown in Fig. 4 C. Neither BLE-treatment nor DMSO alone have a significant effect on the maximum volume. For mild dilutions, $C = 0.7$, nocodazole has no effect, consistent with the fact that neurites swell like a perfect osmometer with 25% dead volume.

Importantly, the cytoskeleton disrupting drugs do not affect the ability of the neurite to perform RVD. As can be seen in Fig. 4 A, the volume fully relaxes back to its initial value. Further evidence can be found in the Supplementary Material.

The effect of temperature: Arrhenius behaviour.

We now address the influence of temperature in the dynamics of volume regulation. For simplicity, we describe the recovery phase by fitting single exponentials. As shown in Fig. 5, lowering the temperature from 35 to 15°C slows down the volume dynamics by an order of magnitude. The dashed line is an Arrhenius-like equation $\tau \propto 1/k \propto e^{\frac{\Delta G}{RT}}$, where k depends on temperature as the rate constant of a thermally-activated process. This yields an activation energy $\Delta G \sim 30$ kT, a typical order of magnitude for biological processes (42). The well-defined Arrhenius trend is consistent with the idea that ion channels are responsible for RVD.

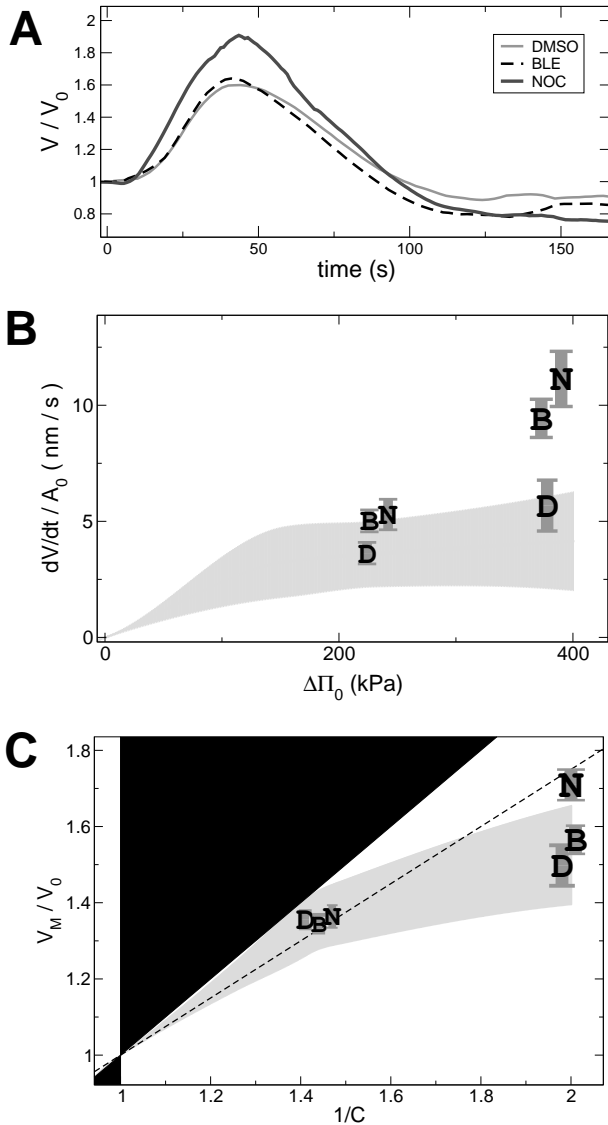


Figure 4: **A:** Comparison of different drug treatments. Each curve is a different neurite. All experiments were performed at temperature $T = 33^\circ\text{C}$ and dilution $C = 0.5$. Grey shaded line: DMSO control. Dashed line: BLE. Black solid line: NOC. **B:** Swelling speed \dot{V}_0/A_0 as a function of the initial osmotic pressure difference $\Delta\Pi_0$, for temperatures 33–36°C. D: DMSO control ($n = 5$ for $C = 0.5$, $n = 14$ for $C = 0.7$). B: blebbistatin ($n = 7$, $n = 13$). N: nocodazol ($n = 8$, $n = 14$). The grey region is a guide to the eye, corresponding to the experiments without drugs shown in Fig. 3 A. Data for all drugs is shown as arithmetic mean \pm S. E. **C:** Maximum relative volume V_M/V_0 as a function of the osmotic pressure difference $\Delta\Pi$ in presence of cytoskeleton-disrupting drugs. The grey region corresponds to the data without drugs in Fig. 3 B.

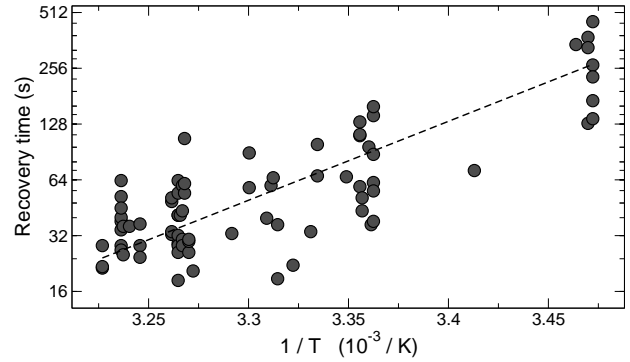


Figure 5: Recovery time as a function of inverse temperature $1/T$. The dashed line is a least-squares fit to an Arrhenius form $\tau \propto e^{\Delta G/RT}$.

Beading

When neurites are subjected to strong hypoosmotic shocks they undergo a shape transformation by developing a periodic array of swellings akin to beading of axons (43). We observe this in chick dorsal root ganglia (DRG) neurons as well as PC12 neurites Fig. 6. This peristaltic deformation, resembles that formed in nerves subjected to induced stretch injuries (31, 32, 44) and that observed after traumatic injuries to the brain (43). The dynamics of bead formation and the mechanism has been investigated recently using the osmotic shock technique (20) and shown to be similar to the pearling instability observed in synthetic membrane tubes under tension (45, 46). Here, we provide direct evidence correlating neurite tension and bead formation and describe the role of cytoskeletal components in this process.

We begin by listing the main features of osmotic shock induced beading. For a given radius of the neurite, there is a critical hypoosmotic shock below which the shape remains cylindrical during the entire volume evolution, and above which a transient peristaltic modulation is observed. This is about $C = 0.5$ at 37°C and about $C = 0.7$ at 25°C for an initial neurite radius of $0.7 \mu\text{m}$. Beading and recovery cycles (for mild shocks) can be repeated up to five times in the same neurite, after which neurites tend to detach from the substrate. Also transport of organelles can be observed during and after beading and recovery. This suggests that mild osmotic shocks leading to beading and recovery causes no permanent damage to the neurites. On the contrary, strong shocks ($C \geq 0.5$) often lead to strongly modulated beaded shapes with no recovery for several tens of minutes. Extreme shocks cause neurites to burst with organelles spewing out, corroborating a build up of membrane tension. Finally, no beading is observed

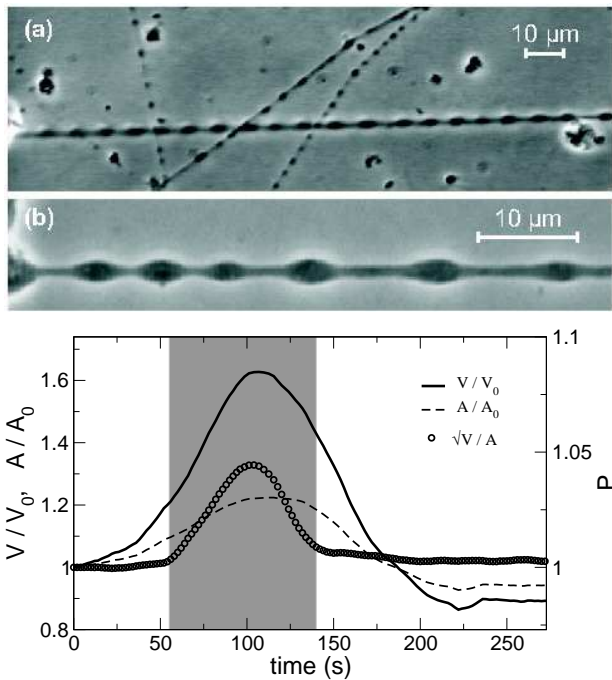


Figure 6: **Top:** Swelling-induced pearling instability. **a:** Chick-embryo neurons. **b:** PC12 neurites at a higher magnification. **Bottom:** Pearling instability. Relative volume V/V_0 , area A/A_0 and shape parameter $\sqrt{V/V_0}/(A/A_0)$ as a function of time. Imposing a fast hypoosmotic shock at dilution $C = 0.5$ and temperature 33°C increases membrane tension and leads to a shape instability. The instability vanishes before the volume recovers.

during hyperosmotic shocks, irrespective of the magnitude.

Axonal tension causes beading. The flow chamber technique has been used recently to quantitatively study the evolution of neurite tension in response to drag forces and to demonstrate active contractile responses in neurites (47). This is performed by imposing a constant, laminar flow perpendicular to the neurite generating a drag force. It has been shown that PC12 neurites as well as axons are viscoelastic (12) and respond to a stretching force via a relaxation process with a characteristic timescale. Under the influence of a flow induced drag force the neurite takes the form of a catenary and elongates until it reaches a final equilibrium shape (47) (see Fig. 7 $t=300\text{s}$). The resulting strain gives a measure of the tension in the axon. Fig. 7 shows snapshots of the neurite taken at various stages during an osmotic shock experiment. Under the influence of the flow the neurite attains an equilibrium catenary shape within about a minute. When the flow is switched from the normal medium to a diluted one, keeping the flow rate the same, the neurite shortens until it

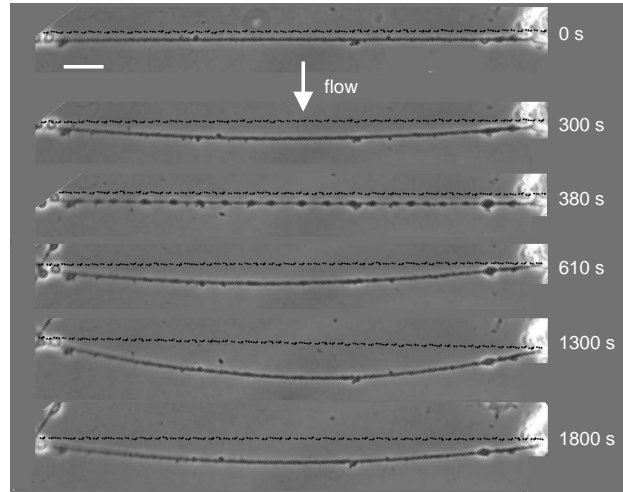


Figure 7: Neurite deformations induced by the combined effect of a constant laminar flow perpendicular to the neurite and different osmotic conditions. The temperature is 25°C and $C_e = 0.7C_0$. The sequence of events is as follows: laminar flow is started at $t = 20\text{ s}$ and the neurite allowed to undergo viscoelastic relaxation and attain a steady state, a hypoosmotic shock is applied at $t = 320\text{ s}$ by introducing dilute medium, the neurite is allowed to undergo volume and shape relaxation, normal medium is reintroduced after the volume has relaxed (hyperosmotic shock) at $t = 1200\text{ s}$, the neurite is again allowed to undergo volume relaxation. The flow rate is constant throughout the experiment. The dashed lines are for comparison of curvature. The larger the average curvature of the catenary, the smaller the tension in the neurite (47).

becomes almost straight. The beading sets in during this straightening phase and the maximum beading amplitude occurs when the neurite is straight ($t=380\text{s}$ in Fig. 7). Subsequently there is a relaxation process in which the beading amplitude begins to decay and the flow-induced curvature increases. When a hyperosmotic shock is applied after the first volume relaxation process ($t=1200\text{s}$ in Fig. 7) the neurite curvature begins to increase as the neurite shrinks and subsequently decreases to almost its normal value with a timescale very much comparable to the volume recovery time. These observations clearly demonstrates that the neurite tension and the volume changes induced by osmotic treatments are correlated.

Beading mechanism. The physical mechanism for bead formation is as follows (20). After applying an osmotic shock the neurite volume increases as discussed above. This results in a corresponding expansion of the measured area $A(t)$ as shown in Fig. 6. This stretching of the membrane causes an increase in the tension of the outer membrane and hence an increase in the surface energy, $F_s = \sigma(A(t) - A_0)^2/A_0$. The increase in

volume also costs bulk elastic energy due to the deformations caused in the cytoskeletal network, which we will consider below later.

It can be shown (46) that at any instant t , for a volume $V(t)$, a peristaltically modulated shape with

$$r(t, z) = r_0 + \epsilon(t) \sin(qz)$$

has a lower average surface area compared to a cylinder with the same instantaneous volume $V(t)$, provided the wavelength $\lambda > 2\pi r_0$. For small amplitudes, the relative area gain can be obtained as

$$\delta S/S = \epsilon(\tilde{q}^2 - 1)/(4r^2),$$

where S is the surface area and $\tilde{q} = 2\pi r/\lambda$. This can be seen in Fig. 6. The ratio $\sqrt{V(t)}/A(t)$ (note: the average volume and area are computed for unit length) increases when the peristaltic mode grows. This quantity is a constant for all cylinders irrespective of radius. An increase in $\sqrt{V(t)}/A(t)$ from this constant value indicates a decrease in area for the peristaltic shape as compared to a cylinder with identical volume. In other words, the neurite is able to reduce its interfacial energy by adopting a peristaltic shape instead of a cylindrical one. As mentioned earlier any deformation costs bulk elastic energy due to the cytoskeletal elasticity. Unlike the surface free energy, the bulk elastic free energy is always positive for peristaltic modes compared to a cylinder of same volume (it costs bulk energy to expand as well as compress regions along the neurite). Therefore, there is a competition between the surface energy and bulk energy which determines the preferred shape, giving rise to a critical tension. A rough expression for the critical tension can be obtained by comparing the average bulk energy per unit length of a cylinder Er_c^2 , where E is the elastic modulus of the cytoskeleton, and the corresponding surface energy σr_c . This gives a critical tension $\sigma_c = Er_c$, above which the surface contribution dominates. As seen in experiments, the critical tension needed to destabilise the cylinder increases with neurite radius. Analogous shape transformations observed in membrane tubes, triggered by application of laser tweezers (45, 46), and in cell protrusions after treatment with latrunculins (48) have been analysed in a similar fashion.

The above mentioned expression for relative gain in area shows that reduction in area increases with wavelength of the perturbation, giving a maximum area gain for $\lambda = L/2$, L the length of the neurite. Clearly, the observed value of λ is much shorter than and independent of the neurite length, but increases linearly with radius. A

simple minded argument for this is as follows. Any perturbation with a wavelength λ generates a pressure difference given by the Laplace law, the pressure difference p balanced by the membrane tension σ . In the case of the axisymmetric modes there are two principal curvatures: that with a curvature radius equal to the neurite radius $r(z)$, and that corresponding to the peristaltic deformation along the z -axis, with a curvature radius $1/\partial_z^2 r(z)$. For large wavelengths, $\lambda \gg \epsilon$, the latter can be ignored. The pressure difference in between the crest and the trough of a peristaltic mode can be written in the small amplitude limit ($\epsilon \ll r$) as

$$\Delta p = \sigma(1/r_{crest} - 1/r_{trough}) \simeq -\sigma\epsilon/r^2.$$

As indicated by the negative sign, this is an unstable flow: the pressure difference will drive water from the troughs into the crests, thereby increasing the perturbation amplitude ϵ . The flow rate and hence the growth of a given mode is in general proportional to the driving force

$$\Delta p/\lambda \sim \sigma\epsilon/\lambda r^2.$$

Shorter wavelength modes are thus faster to grow than longer wavelength ones. However, for very short wavelengths the curvature along the neurite axis becomes important. The respective pressure difference is given by $\Delta p = \sigma\partial_z^2 r(z) \simeq \sigma\epsilon/\lambda^2$. In contrast to the previous case, here the cylindrical state is stable: water flows from the crests into the troughs (which have a “negative” pressure) making the perturbation vanish. Moreover, the dependence of the flow rate on the wavelength is more pronounced,

$$\Delta p/\lambda \sim \sigma\epsilon/\lambda^3.$$

Therefore for very small wavelengths the stabilizing flow driven by the curvature along z always dominates, and there is no instability anymore. We conclude that there is a fastest mode at an intermediate, non-zero wavelength. This can be shown to be $\lambda \simeq 9.2r$ (49). In the very dawn of linear stability analysis, this argument was applied to the case of water jets by Lord Rayleigh (50, 51).

THEORY

We model volume regulation in neurites taking into account both mechanical and osmotic driving forces. The neurite is characterised by its volume, $V(t)$, and the internal amounts of ionic species, $n_i(t)$. For simplicity we consider only potassium and chloride, by large the most

important osmolites inside the cell. Since due to electroneutrality the flows of Cl^- and K^+ are coupled,

$$\dot{n}_{\text{Cl}} = \dot{n}_{\text{K}} ,$$

one of the two concentrations can be eliminated. The two variables of our model are the adimensional quantities

$$\mathcal{V} = V(t) / V_0 \quad (3)$$

$$\mathcal{N} = n_{\text{Cl}}(t) / n_{\text{Cl}}(0) . \quad (4)$$

The flow of water through the membrane (1) is given by

$$\dot{V} = AL_p(\Delta\Pi - \Delta p) , \quad (5)$$

where A is the neurite area, L_p the hydraulic permeability, Δp the hydrostatic pressure, and the osmotic pressure difference is given by

$$\Delta\Pi \simeq RT \sum_i (n_i/V - c_i^{\text{ex}})$$

in terms of external c_i^{ex} and internal osmolite concentrations n_i/V . The typical relaxation time for the volume is

$$\tau_V = \frac{V_0}{AL_p\Pi_0} ,$$

where $\Pi_0 = RTC_0 \simeq 700$ kPa the osmotic pressure of normal medium. Taking 10^{-14} m Pa $^{-1}$ s $^{-1}$ for the permeability (from Fig. 3 A) we obtain $\tau_V = 50$ s.

We model ion movement with a passive K^+ - Cl^- co-transport following Ref. (3), neglecting the effect of ion pumps since these are not relevant for the short-term RVD response. Chloride flux is given by the difference in chemical potentials,

$$\dot{n}_{\text{Cl}} = -ARTG \log \left(\frac{n_{\text{Cl}}n_{\text{K}}}{V^2} \frac{1}{C^2c_{\text{Cl}}c_{\text{K}}} \right) . \quad (6)$$

We model the RVD response following the standard assumption of a volume-dependent permeability (2). The permeability G must be zero at the initial volume V_0 and non-zero at a significant departure. We decompose

$$G(\mathcal{V}) = |G| g(\mathcal{V}) ,$$

into a typical order of magnitude $|G|$ and an adimensional function $g(\mathcal{V})$. For the chloride relaxation time

$$\tau_{\text{Cl}} = \frac{V_0 c_{\text{Cl}}^{\text{in}}}{ART|G|} ,$$

we expect a value of 10–100 s taking typical values for ion conductivities (1). The volume-dependent permeability function $g(\mathcal{V})$ jumps from zero to a finite value at a

critical threshold volume; otherwise its form is not known and different expressions have been used in the literature (3, 17). In our experiments the critical volume is about $1.2 V_0$, as can be seen in Fig. 2. We obtain good results with the simple expression

$$g = \theta(\mathcal{V}/1.2) \mathcal{V} ,$$

where $\theta()$ is the step function.

Finally, assuming external ion concentrations to jump instantaneously at time $t = 0$ from $c_i^{\text{ex}}(0)$ to $Cc_i^{\text{ex}}(0)$ the full system can be written as

$$\dot{\mathcal{V}} = \frac{1}{\tau_V} \left(\frac{1 + 2\phi(\mathcal{N} - 1)}{\mathcal{V}} - \frac{\Delta p}{\Pi^0} - C \right) \quad (7)$$

$$\dot{\mathcal{N}} = -\frac{g(\mathcal{V})}{\tau_{\text{Cl}}} \log \left(\frac{\alpha \mathcal{N}^2 + (1 - \alpha) \mathcal{N}}{\beta C^2 \mathcal{V}^2} \right) \quad (8)$$

with the parameters

$$\phi = c_{\text{Cl}}^{\text{in}} / C_0 \quad (9)$$

$$\alpha = c_{\text{Cl}}^{\text{in}} / c_{\text{K}}^{\text{in}} \quad (10)$$

$$\beta = c_{\text{Cl}}^{\text{ex}} c_{\text{K}}^{\text{ex}} / c_{\text{Cl}}^{\text{in}} c_{\text{K}}^{\text{in}} . \quad (11)$$

Taking the following physiological values for the ion concentrations (1)

$$c_{\text{Cl}}^{\text{in}} = 80 \text{ mM}$$

$$c_{\text{K}}^{\text{in}} = 150 \text{ mM}$$

$$c_{\text{Na}}^{\text{in}} = 15 \text{ mM}$$

$$c_{\text{Cl}}^{\text{ex}} = 80 \text{ mM}$$

$$c_{\text{K}}^{\text{ex}} = 6 \text{ mM}$$

$$c_{\text{Na}}^{\text{ex}} = 110 \text{ mM} ,$$

the adimensional constants become $\phi = 0.25$, $\beta \simeq 0.05$, and $\alpha \simeq 0.5$.

Zero pressure model. The standard assumption in modelling volume regulation is to set the hydrostatic pressure to zero (3),

$$\Delta p = 0 .$$

With this ansatz we can solve the equations for the volume response $\mathcal{V}(t)$. As shown in Fig. 8, the model reproduces the timescales for swelling and recovery as well as the maximum volume. Interestingly it reproduces the ‘‘undershoot’’ at $C = 0.5$ (see Fig. 2). However, the dependence of the swelling rate on osmotic pressure is clearly off. The model gives a linear response—a feature intrinsic to any volume-dependent permeability—whereas experiments show a nonlinear one (Fig. 3 A).

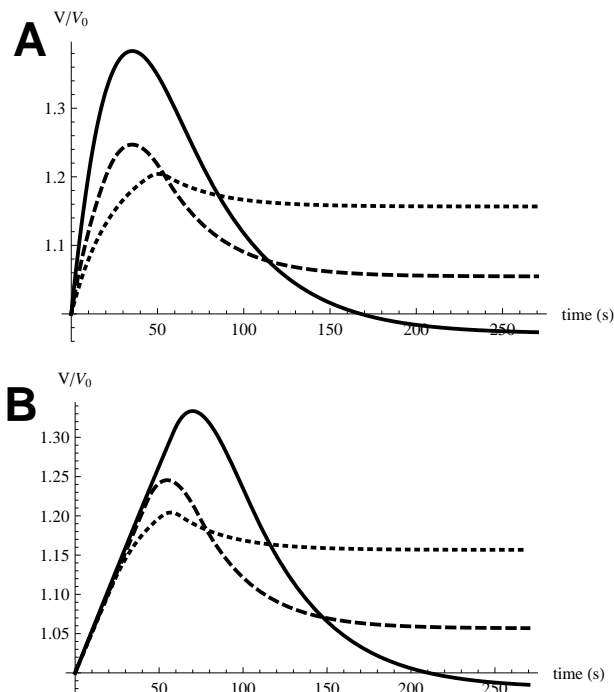


Figure 8: **A:** zero pressure model for dilutions 80% (dotted line), 70% (dashed line) and 50% (solid line). **B:** adding nonlinear friction as given by Eq. 12 reproduces the trend during the swelling phase. Compare to Figs. 2,6

Viscoelastic model. As shown by our experiments combining hypoosmotic shocks and drag forces (Fig. 6), neurites develop tension while swelling. This suggests that the nonlinear response observed in experiments may come from a nonlinear mechanical response, a ubiquitous feature of cells with structured cytoskeleton (52). We therefore assume that the pressure difference Δp is not zero, but depends on the swelling rate as expected for a viscoelastic element. To reproduce Fig. 3 A, we assume that neurites swell at zero pressure below a critical rate but encounter internal friction for rates larger than a critical value Ω . This can be written as

$$\Delta p = \begin{cases} 0 & \text{for } |\dot{V}| < \Omega \\ \eta \text{ sign}(\dot{V}) (|\dot{V}|/\Omega - 1) & \text{for } |\dot{V}| > \Omega \end{cases} \quad (12)$$

where Ω is the maximal rate of change of volume at which the neurite can swell without tension, corresponding to about $5 \cdot 10^{-3} \text{ s}^{-1}$ in our experiments, and η is the friction scale, about 2 MPa.

As shown in Fig. 8, with this ansatz the model reproduces the essentially constant swelling rate observed in experiments. The nonlinear friction slows down both swelling and recovery. Interestingly, the peculiar triangular shape of the curves at $C = 0.5$ is much closer to

that of experiments (compare to Fig. 2).

DISCUSSION

Microtubules mechanically slow down swelling. The initial response of neurites to hypo- as well as hyperosmotic shocks is a strongly nonlinear function of the external osmotic pressure. Remarkably, this response becomes much simpler after microtubule disruption: neurites behave as perfect-osmometers, and the swelling rate increases linearly with osmotic shock strength. The simplest explanation is that microtubules slow down the initial volume change by mechanically opposing the hydrostatic pressure difference. This is not exactly an elastic response but rather a (nonlinear) viscous one which depends crucially on the swelling rate. This mechanical role of microtubules may come as a surprise, as they are in general irrelevant for the (passive) mechanical response of cells. In neurites, however, their structure is different: they are arranged in bundles interconnected by microtubule binding proteins (MBPs). Our results indicate that microtubules are firmly connected to the membrane, either directly by MBPs or through the actin cortex. Interestingly, studies of volume regulation on round PC12 cells without neurites give a different picture. Whereas disruption of the actin cytoskeleton by Cytochalasin B has been reported to increase KCl efflux and diminish extent of swelling (25, 53), disruption of microtubules has no effect on RVD (25). This is consistent with our conclusion of a mechanical role for microtubuli, since these are organised very differently in round cells and neurites: in the latter their bundle structure provides a rigid scaffold which can oppose swelling.

The mechanical response of the neurite, as described by Eq. 12, seems to be similar to that of adhering fibroblasts (52, 54). At slow strain rates, forces are low; above a critical strain rate, friction increases and the force becomes much stronger. From our results, writing the critical rate as a strain we get $\dot{V}_0/(r_0 A_0) \sim 5 \cdot 10^{-3} \text{ s}^{-1}$. In single fibroblasts, this is indeed the order of magnitude of the critical strain rate where frictional forces increase (52), which in turn agrees with the timescale of active processes (9, 11). This suggests that changes in cell shape –including swelling– take place at the rate allowed by spontaneous unbinding of cytoskeletal crosslinks, while faster changes are slowed down by friction between cytoskeletal elements.

RVD is osmotically driven. Our results indicate that mechanical tension does not provide the driving force for volume recovery. The pearling modulation vanishes

well before the volume recovers, indicating zero membrane tension during RVD. Moreover, in presence of cytoskeleton-perturbing drugs the volume recovery time τ does not increase, but becomes slightly shorter. This indicates that volume recovery takes place via extrusion of osmolites (3). Indeed, our simple model based on two ionic species suffices to explain the essential features of the volume evolution curves. It captures the broad response and even the tendency to “undershoot” at large dilutions.

RVD follows an Arrhenius trend as a function of temperature. The timescales involved in the volume responses are temperature dependent. The relaxation time is about an order of magnitude more temperature dependent than the swelling/shrinking rate, showing an exponential reduction as the temperature is increased. Thus the ability of the cell to respond to and negate perturbations to its volume improves drastically as the temperature approaches the normal physiological values. Due to this reason the neurites are able to withstand strong hypoosmotic-shocks at higher temperatures when the same shock would have made them rupture at a slightly lower temperature.

A dynamic picture of stretch injury. Similar shape transformations have been observed in nerves under the name of “beading” as a response to stretch injury (31, 32). Interestingly, electron microscopy observations of the ultrastructure of stretch-beaded nerves show that microtubules are splayed out in the beads (44), consistent with our picture of a mechanical connection between microtubules and the membrane. The shapes of beaded nerves have been interpreted as equilibrium shapes with a constant curvature (31); however, our results offer an alternative explanation, namely that the shape is given by the fastest growing mode at the time of the increase in tension. If so, the shape of beaded nerves would not simply follow from structural properties (as expected for an equilibrium shape) but would also be defined by the precise way stretch-injury takes place, i.e., the rate and extent of loading. Future studies may address this question in detail.

Conclusions

Neurites respond to sudden osmotic pressure changes with a fast volume regulation response. The initial phase is characterised by a nonlinear dependence of swelling rate on the initial osmotic pressure. Cytoskeletal perturbation, especially microtubule disruption, accelerates swelling and increases the maximum volume reached, but does not affect the relaxation phase. Taking our results to-

gether, we propose that mechanical forces due to the nonlinear viscosity of the cytoskeleton slow down the initial phase of change of volume. This may provide instantaneous integrity to the neurite while osmotic mechanisms “warm up”.

Acknowledgements

Experiments were performed at the Universität Bayreuth, Germany, with the generous financial support of Albrecht Ott. We thank Osvaldo Chara, Pablo Schwarzbaum, Karina Alleva and Wolfram Hartung for helpful discussions.

References

1. Weiss, T., 1996. Cellular Biophysics. MIT Press.
2. Lang, F., G. Busch, M. Ritter, H. Völkl, S. Waldeger, E. Gulbins, and D. Häussinger, 1998. Functional significance of cell volume regulatory mechanisms. *Physiol. Reviews* 78:247.
3. Hernandez, J., and E. Cristina, 1998. Modelling cell volume regulation in nonexcitable cells: the roles of the Na⁺ pump and of cotransport systems. *Am. Physiol. Soc.* C1067.
4. MacKnight, A. D. C., 1987. Volume Maintenance in Isosmotic Conditions. *In* R. Gilles, A. Kleinzeller, and L. Bolis, editors, Cell Volume Control: Fundamental and comparative aspects in animal cells. Academic Press, San Diego, 3–43.
5. Bray, D., 2001. Cell Movements: from molecules to motility. Garland Publishing, Inc., New York, 2nd edition.
6. Alberts, B., D. Bray, J. Lewis, M. Raff, K. Roberts, and J. D. Watson, 1994. Molecular Biology of the Cell. Garland Publishing, Inc., New York, 3rd edition.
7. Janmey, P. A., 1998. The cytoskeleton and cell signaling: component localization and mechanical coupling. *Physiol. Rev.* 78:763–781.
8. Fabry, B., G. N. Maksym, J. P. Butler, M. Glogauer, D. Navajas, and J. J. Fredberg, 2001. Scaling the microrheology of living cells. *Phys. Rev. Lett.* 87:148102.

9. Thoumine, O., and A. Ott, 1997. Time scale dependent viscoelastic and contractile regimes in fibroblasts probed by microplate manipulation. *J. Cell. Sci.* 110:2109–2116.
10. Fernández, P., P. A. Pullarkat, and A. Ott, 2006. A master relation defines the nonlinear viscoelasticity of single fibroblasts. *Biophys. J.* 90:3796–3805.
11. Pullarkat, P. A., P. A. Fernández, and A. Ott, 2007. Rheological properties of the Eukaryotic cell cytoskeleton. *Phys. Rep.* 449:29–53.
12. Bernal, R., P. A. Pullarkat, and F. Melo, 2007. Mechanical properties of axons. *Phys. Rev. Lett.* 99:018301.
13. Henson, J., 1999. Relationships between the Actin Cytoskeleton and Cell Volume Regulation. *Microscopy research and technique* 47:155–162.
14. Kleinzeller, A., 1965. The volume regulation in some animal cells. *Arch. Biol.* 76:217–232.
15. Cantielo, H., 1997. Role of actin filament organization in cell volume and ion channel regulation. *J. Exp. Zoology* 279:425.
16. Mills, J., 1987. The Cell Cytoskeleton: Possible Role in Volume Control. In R. Gilles, A. Kleinzeller, and L. Bolis, editors, Cell volume control: fundamental and comparative aspects in animal cells. Academic Press, Inc., San Diego, 75–101.
17. Strieter, J., J. L. Stephenson, L. G. Palmer, and A. M. Weinstein, 1990. Volume-activated chloride permeability can mediate cell volume regulation in a mathematical model of a tight epithelium. *J. Gen. Physiol.* 96:319–344.
18. Strange, K., 2004. Cellular volume homeostasis. *Adv. Physiol. Educ.* 28:155–159.
19. Downey, G., S. Grinstein, A. Sue-A-Quan, B. Czaiban, and C. Chan, 1995. Volume Regulation in leukocytes: requirement for an intact cytoskeleton. *J. Cell Physiol.* 163:96–104.
20. Pullarkat, P., P. Dommersnes, P. Fernández, J.-F. Joanny, and A. Ott, 2006. Osmotically induced shape transformations in axons. *Phys. Rev. Lett.* 96:048104.
21. Wan, X., J. Harris, and C. Morris, 1995. Responses of neurons to extreme osmomechanical stress. *J. Memb. Biol.* 145:21–31.
22. Heubusch, P., C. Jung, and F. Green, 1985. The osmotic response of human erythrocytes and the membrane cytoskeleton. *J. Cell. Physiol* 122:266–272.
23. Suchyna, T., S. Besch, and F. Sachs, 2004. Dynamic regulation of mechanosensitive channels: capacitance used to monitor patch tension in real time. *Phys Biol* 1:1.
24. D'Alessandro, M., D. Russell, S. M. Morley, A. M. Davies, and E. Birgitte Lane, 2002. Keratin mutations of epidermolysis bullosa simplex alter the kinetics of stress response to osmotic shock. *J. Cell Sci.* 115:4341–4351.
25. Cornet, M., E. Delpire, and R. Gilles, 1988. Relations between cell volume control, microfilaments and microtubules networks in T2 and PC12 cultured cells. *J. Physiol. Paris* 83:43–49.
26. Light, D., A. Attwood, C. Siegel, and N. Baumann, 2003. Cell swelling increases intracellular calcium in *Necturus* erythrocytes. *J. Cell Sci.* 116:101–109.
27. Arora, P., K. Bibby, and C. McCulloch, 1994. Slow oscillations of free intracellular calcium ion concentration in human fibroblasts responding to mechanical stretch. *J. Cell. Physiol.* 161:187–200.
28. Guilak, F., R. Zell, G. Erickson, D. Grande, C. Rubin, K. McLeod, and H. Donahue, 1999. Mechanically induced calcium waves in articular chondrocytes are inhibited by gadolinium and amiloride. *J. Orthop. Res.* 17:421–429.
29. Greene, L., and A. Tischler, 1976. Establishment of a noradrenergic clonal line of rat adrenal pheochromocytoma cells which respond to nerve growth factor. *Proc. Natl. Acad. Sci. USA* 73:2424–2428.
30. Roger Jacobs, J., and J. Stevens, 1986. Changes in the organization of the neuritic cytoskeleton during nerve growth factor-activated differentiation of PC12 cells: a serial electron microscopic study of the development and control of neurite shape. *J. Cell Biol.* 103:895–906.
31. Markin, V., D. Tanelian, R. Jersild, Jr., and S. Ochs, 1999. Biomechanics of stretch-induced beading. *Biophys. J.* 76:2852–2860.
32. Ochs, S., R. Pourmand, and R. Jersild, Jr., 1996. Origin of beading constrictions at the axolemma:

- presence in unmyelinated axons and after β, β' -iminodipropionitrile degradation of the cytoskeleton. *Neuroscience* 70:1081–1096.
33. Drexler, H. G., W. Dirks, W. R. A. F. MacLeod, H. Quentmeier, K. G. Steube, and C. C. Uphoff, 2001. DSMZ Catalogue of Human and Animal Cell Lines. Braunschweig.
 34. Greene, L., M. Sobeih, and K. Teng, 1991. Methodologies for the culture and experimental use of the PC12 rat pheochromocytoma cell line. In G. Banker, and K. Goslin, editors, *Culturing Nerve Cells*. MIT Press, Cambridge, 207–226.
 35. De Brabander, M., R. Van de Veire, R. Aerts, M. Borgers, and P. Janssen, 1976. The effects of methyl[5-(2-thienylcarbonyl)-1H-benzimidazol-2-yl]carbamate (R 17 934, NSC 238159), a new synthetic antitumoral drug interfering with microtubules, on mammalian cells cultured in vitro. *Cancer Res.* 36:905–916.
 36. Straight, A. F., A. Cheung, J. Limouze, I. Chen, N. J. Westwood, J. R. Sellers, and T. J. Mitchison, 2003. Dissecting temporal and spatial control of cytokinesis with a Myosin II inhibitor. *Science* 299:1743–1747.
 37. van Hoek, A. N., M. D. de Jong, and C. H. van Os, 1990. Effects of dimethylsulfoxide and mercurial sulfhydryl reagents on water and solute permeability of rat kidney brush border membranes. *Biochim.Biophys.Acta* 1030:203–210.
 38. Maric, K., B. Wiesner, D. Lorenz, E. Klussmann, T. Betz, and W. Rosenthal, 2001. Cell volume kinetics of adherent epithelial cells measured by laser scanning reflection microscopy: determination of water permeability changes of renal principal cells. *Biophys.J.* 80:1783–1790.
 39. Huster, D., A. Jin, K. Arnold, and K. Gawrisch, 1997. Water permeability of polyunsaturated lipid membranes measured by ^{17}O NMR. *Biophys.J.* 73:855–864.
 40. Lucio, A., R. Santos, and O. Mesquita, 2003. Measurements and modeling of water transport and osmoregulation in a single kidney cell using optical tweezers and videomicroscopy. *Phys. Rev. E* 68:041906.
 41. Fernández, P., 2006. Mechanics of living cells: nonlinear viscoelasticity of single fibroblasts and shape instabilities in axons. Ph.D. thesis, Universität Bayreuth.
 42. Blumenfeld, L. A., and A. N. Tikhonov, 1994. Biophysical thermodynamics of intracellular processes: molecular machines of the living cell. Springer, Berlin.
 43. D. Kilinc, G. G., and K. A. Barbee, 2008. Mechanically-induced membrane perturbation causes axonal beading and localized cytoskeletal damage. *Exp. Neurol.* 212:422–430.
 44. Ochs, S., R. Jersild, Jr., R. Pourmand, and C. Potter, 1994. The beaded form of myelinated nerve fibers. *Neuroscience* 61:361–372.
 45. Bar-Ziv, R., and E. Moses, 1994. Instability and “pearling” states produced in tubular membranes by competition of curvature and tension. *Phys. Rev. Lett.* 73:1392–1395.
 46. Bar-Ziv, R., E. Moses, and P. Nelson, 1998. Dynamic excitations in membranes induced by optical tweezers. *Biophys.J.* 75:294–320.
 47. Bernal, R., F. Melo, and P. A. Pullarkat, 2009. Drag force as a tool to test the active mechanical response of PC12 neurites. *in press in Biophys. J.*
 48. Bar-Ziv, R., and E. Moses, 1999. Pearling in cells: a clue to understanding cell shape. *Proc. Natl. Acad. Sci. USA* 96:10140–10145.
 49. Nelson, P., T. Powers, and U. Seifert, 1995. Dynamic theory of pearling instability in cylindrical vesicles. *Phys. Rev. Lett.* 74:3384.
 50. Rayleigh, L., 1892. On the instability of a cylinder of viscous liquid under capillary force. *Philos.Mag.* 34:195.
 51. Chandrasekhar, S., 1970. Hydrodynamic and hydro-magnetic stability. Dover, New York, 3 edition.
 52. Fernández, P., and A. Ott, 2008. Single cell mechanics: stress stiffening and kinematic hardening. *Phys. Rev. Lett.* 100:238102.
 53. Cornet, M., J. Ubl, and H.-A. Kolb, 1993. Cytoskeleton and ion movements during Volume regulation in cultured PC12 cells. *J. Membrane Biol.* 133:161–170.

54. Fernández, P., L. Heymann, A. Ott, N. Aksel, and P. A. Pullarkat, 2007. Shear rheology of a cell monolayer. *New J. Phys.* 9:419.